ACS Photonics

Article

pubs.acs.org/journal/apchd5

Light Outcoupling from Quantum Dot-Based Microdisk Laser via Plasmonic Nanoantenna

Eduard I. Moiseev,[†] Natalia Kryzhanovskaya,[†,‡] Yulia S. Polubavkina,[†] Mikhail V. Maximov,[†,‡,§] Marina M. Kulagina,[§] Yury M. Zadiranov,[§] Andrey A. Lipovskii,[†,‡] Ivan S. Mukhin,[†,∥] Alexey M. Mozharov,[†,∥] Filipp E. Komissarenko,[†,∥] Zarina F. Sadrieva,[∥] Alexander E. Krasnok,[∥,⊥] Andrey A. Bogdanov,*[,∥,§] Andrei V. Lavrinenko,[∥] and Alexey E Zhukov[†,‡]

[†]St. Petersburg Academic University, 8/3 Khlopina, St. Petersburg 194021, Russia

[‡]Peter the Great St. Petersburg Polytechnic University, St. Petersburg 195251, Russia

[§]Ioffe Institute, 26 Polytechnicheskaya, St. Petersburg 194021, Russia

[∥]ITMO University, St. Petersburg 197101, Russia

[⊥]Department of Electrical and Computer Engineering, The University of Texas at Austin, Austin, Texas 78712, United States

Supporting Information

ABSTRACT: Microdisk lasers demonstrate high performance and low threshold characteristics due to supporting of whispering gallery modes with a high quality factor. One of the challenging problems impeding some practical applications of whispering gallery mode lasers is that they have isotropic emission predominantly lying in the plane of the cavity. In this work, we present a novel method that provides both enhancement of the laser emission and modifies its directivity, making the vertical direction favorable. Electromagnetic energy outcouples from the cavity through the platinum−carbon plasmonic wire nanoantenna grown by electron-beam assisted deposition right up the side wall of the cavity. Evanescent field of whispering gallery mode excites surface plasmon polariton which propagates along the nanoantenna and scatters at its tip. We demonstrate 20× enhancement of the dominant mode intensity with 24 dB of side mode suppression increment without essential worsening of the *Q*-factor which remains over 3×10^4. The proposed approach of the efficient control over the spectrum, directivity, and emission efficiency from microdisk lasers could be very promising for many practical applications from telecommunication technologies to biosensing.

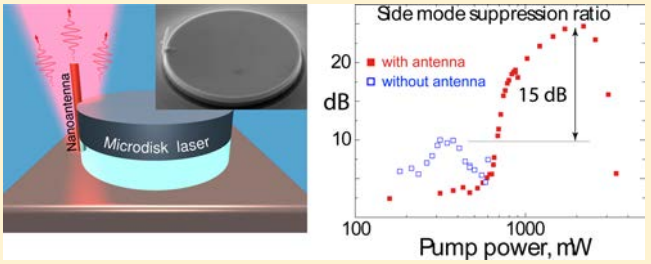

KEYWORDS: *QD laser, single-mode lasing, WGM, near IR, electron beam induced deposition, optical nanoantenna, plasmonic nanoantenna, SPP*

Plasmonic optical nanoantennas offer a large number of applications due to focusing and confining electromagnetic waves into nanoscale volumes by employing the unique properties of surface plasmon polaritons. These properties bring about an enhancement of light-matter interaction, and an ability to form a desired radiation pattern, which opens new unique opportunities for designing of microscopic optical sources.[1−5] Currently, plasmonic nanoantennas are used in microscopy, spectroscopy,[6] nonlinear optics,[7−9] wavefront engineering,[10,11] and biological applications.[12] Nanoantennas are also used for collection of an emitted light in the far field.[6,13−15]

In turns, optical microcavities supporting high-*Q* whispering gallery modes (WGMs) are prominent for ultralow-threshold microlaser applications. Due to the axial symmetry of a circular cavity, light emission is isotropic in the plane of the cavity and the efficiency of the light outcoupling is very low (0.02−0.1%).[16] In order to increase the outcoupling efficiency and directivity of light emission from microdisks/microrings, various types of defects have been proposed, such as a point scatterer,[17] a linear defect,[18,19] a finite size air hole or dielectric nanoparticle at the top face of the cavity.[20,21] A general disadvantage of this method is that defects spoil the *Q*-factor of the cavities. Alternatively, radiation from WGM cavities can be outcoupled via evanescent fields using tapered fibers, waveguides, or prisms.[22−26] Potentially, these techniques are very promising for many on-chip applications; however, they require very precise fabrication since the coupling strength has an exponential dependence on the distance between the cavity and the waveguide.[27,28] Another approach to obtain directional emission is to deform the shape of the cavity, thereby breaking its rotational symmetry. Using this approach, room temperature operation of optically pumped microlasers[29] and low-temper-

Received: August 1, 2016

DOI: 10.1021/acsphotonics.6b00552
ACS Photonics XXXX, XXX, XXX−XXX

ature (20 K) lasing in electrically pumped lasers[30] have been demonstrated. High in-plane emission directivity was achieved in midinfrared laser with an elliptical cavity and a wavelength-size notch defect.[31] However, in many areas of technology such as optical communications, optical neural networks, and optical signal processing it is necessary to increase light emission in the vertical direction.[32−35] For this purpose, it seems reasonable to use vertical-cavity surface-emitting lasers (VCSELs).[36] Indeed, VCSELs are specifically designed to provide vertical emission. They have many advantages and are widely used for many applications, especially in the optical communication industry.[37,38] However, some applications, as sensing of single molecules, need very narrow spectral lines,[39] which could not be obtained with VCSELs. In this sense, *Q*-factor of WGM lasers is a distinct advantage; it can reach values up to 10^{10} or even higher.[40]

For practical applications it is also desired to have a single-frequency lasing. However, microring and microdisk lasers typically demonstrate multifrequency lasing on WGM of different azimuthal and radial orders (see, e.g., refs 41 and 42). In order to enhance the single frequency lasing, various methods have been proposed,[43−45] which are usually based on the suppression of the undesired modes, whereas the intensity of a dominant mode remains unchanged or even degrades.

In this work, we use a plasmonic (Pt−C) wire nanoantenna for mode selection and enhancement of a radiation emission in vertical direction from quantum dot based microdisk laser (see Figure 1). The Pt−C nanoantenna was grown by electron-beam assisted deposition right up the side wall of the microcavity. We demonstrate that the outcoupling of electromagnetic energy occurs through a surface plasmon polariton, which is excited by an evanescent tail of the whispering gallery mode of the cavity, then propagates along the surface of the nanowire and scatters at its tip. This modifies the directivity of the laser emission, making it vertically oriented. We achieved 20 times enhancement of the dominant mode intensity with 24 dB of side mode suppression increment without essential worsening of the *Q*-factor, which remains over 30000. We also observe noticeable breaking of circular symmetry of light emission from the microdisk with nanoantenna.

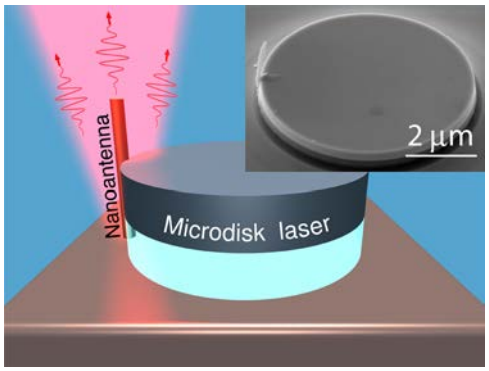

Figure 1. Schematic view of the plasmon nanoantenna for light outcoupling from quantum dot-based microdisk laser. The inset shows the scanning electron microscopy image of 6 μm diameter microdisk with 150 nm wide and 1.3 μm high nanoantenna. The microdisk cavity was fabricated using photolithography and Ar^+ ion beam etching. The wafer was grown using molecular beam epitaxy on a semi-insulating GaAs (100) substrate. The active region is formed by an array of self-organized InAs/InGaAs QDs. The Pt−C nanoantenna was grown by electron-beam-assisted deposition.

SAMPLE, METHODS, AND EXPERIMENT DETAILS

An epitaxial structure was grown by molecular beam epitaxy on an n^+ GaAs(100) substrate. The active region represents 5 layers of self-organized InAs/InGaAs quantum dots (QDs) inserted into a 0.35 μm thick GaAs waveguiding layer cladded with 400 nm thick $Al_{0.98}Ga_{0.02}As$ layer from the substrate side. Owing to the deep localization of charge carriers in QDs, the lateral transport of carriers is inhibited and, as a consequence, their nonradiative recombination at the side wall of the microcavity is suppressed. Spectral position of the quantum dot ground-state transition was located around at 1.28 μm at room temperature. Microdisk resonator was fabricated using photolithography and Ar^+ ion beam etching. The diameter of the microdisks was 6 μm. The $Al_{0.98}Ga_{0.02}As$ bottom cladding layer was selectively oxidized to be transformed into an $(AlGa)_xO_y$ layer to improve the optical confinement.[46]

Nanoantennas were formed directly at the side wall of the cavity by means of electron-beam-induced deposition with $C_9H_{16}Pt$ precursor gas using a Carl Zeiss CrossBeam 1540XB microscope. The precursor gas was injected through a micronozzle into the spatial region of the electron beam focus. The operation pressure in the microscope chamber was 2×10^{-5} mBarr, electron beam diameter, and current was 2−3 nm and 50 pA, respectively, Pt−C nanoantenna growth rate was about 160 nm/s. The fabricated nanoantenna diameter was 150 nm and its height was 1.3 μm. So, the total time of growth was less than 10 s. The nanoantennas formed under such growth conditions have a polycrystalline structure representing a dense array of adjoint Pt nanocrystallites with a size of 2−3 nm inserted into an amorphous carbon matrix. The inset of Figure 1 depicts a microscopic image of the microdisk with a nanoantenna attached to it.

Electrical properties of Pt−C composite material were characterized by resistivity measurement, which was carried out for a Pt−C nanoantenna deposited at the same conditions onto prepatterned metallic (Au) test structure (see inset in Figure 2). The DC current−voltage curve demonstrates Ohmic

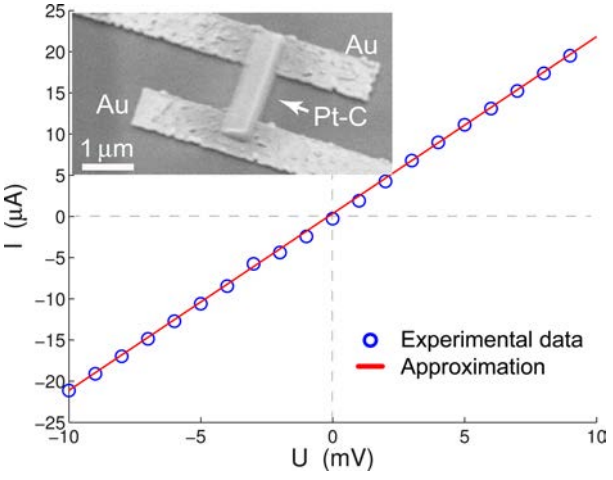

Figure 2. Current−voltage characteristic of Pt−C a nanoantenna. The insets shows electron microscope image of Au contacts with deposited Pt−C nanoantenna used for conductance measurement. The Pt−C nanoantenna was grown by electron-beam assisted deposition.

DOI: 10.1021/acsphotonics.6b00552
ACS Photonics XXXX, XXX, XXX−XXX

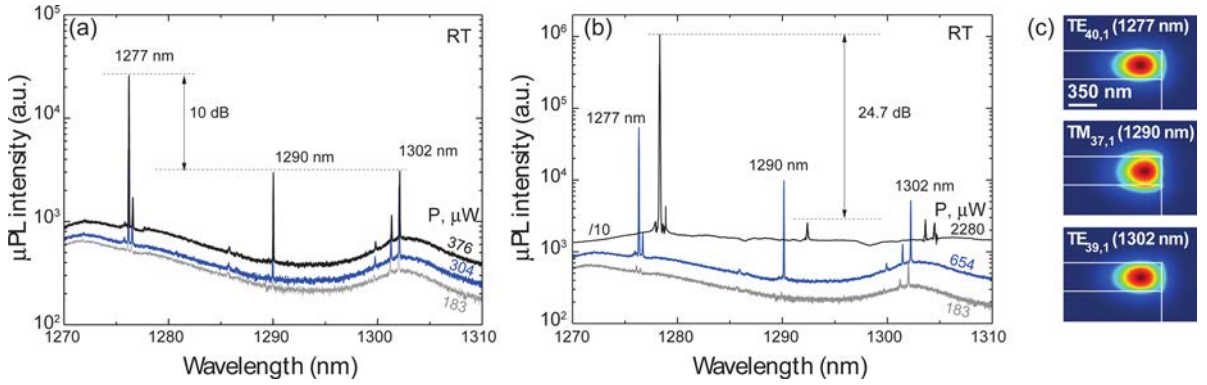

Figure 3. Lasing spectra of the microdisk before (a) and after (b) the nanoantenna deposition taken at room temperature at various pump powers P. The microdisk is pumped by a CW-operating YAG:Nd laser (λ = 532 nm). (c) Distribution of the electric field amplitude |E| for the modes observed in the photoluminescence spectra of the microdisk laser.

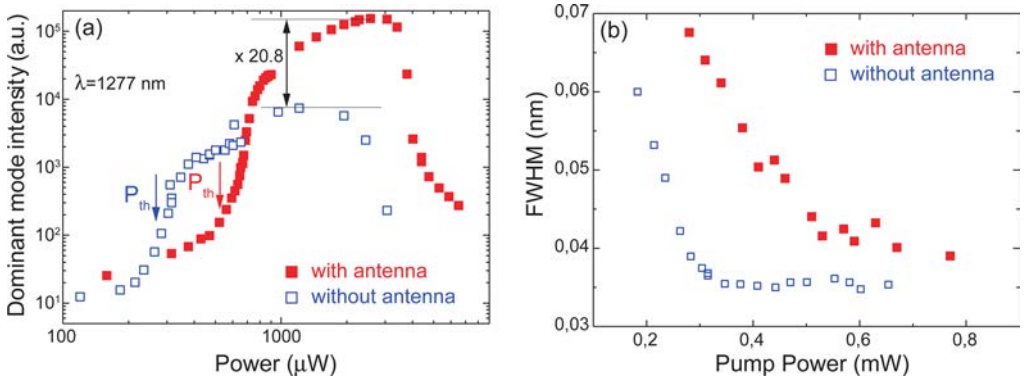

Figure 4. (a) Measured intensity of the dominant mode ($TE_{40,1}$) as a function of pump power for the microdisk with and without the nanoantenna. (b) Line width of the same mode as a function of pump power for the microdisk with and without the nanoantenna.

behavior. The resulting specific resistance is 1.5×10^{-5} Ohm·m, which is higher than the bulk Pt resistivity (10^{-7} Ohm·m), but is within the range of data reported in literature for Pt nanoelectrodes[47,48] and Pt−C wires.[49] It means that the array of nanocrystallites is quite dense and can exhibit plasmonic properties. The relative content of Pt and C in the composite depends on many conditions such as electron beam current, energy of electrons, type of the precursor etc. The Pt−C composites grown at the conditions, similar to those we have, contain from 30 to 70% of Pt.[50−52] The annealing increases the Pt content, however, it could result in serious deformation or even destruction of the wire nanoantenna.[53] To demonstrate that the Pt−C nanoantenna has plasmonic resonances we fabricated samples of single Pt−C nanoantennas and measured their dark-field spectra (see Supporting Information).

For microphotoluminescence (μPL) investigations, a CW-operating YAG:Nd laser (λ = 532 nm) was used. The microdisk was uniformly pumped by the laser using lensed fiber. The samples were characterized at room temperature. A piezo-electrically adjustable objective (Olympus LMPlan IR objective ×100 with NA = 0.8) was used to focus the incident laser beam and to collect the μPL signal from the microresonator. The collected μPL was then analyzed with a 1000 mm monochromator Horiba FHR coupled with a cooled InGaAs CCD array. The system provided a spectral resolution of 0.03 nm for 1200 mm^{-1} grating. The spatial distribution of the emitting light was measured by scanning the sample surface with ×100 Mitutoyo objective using confocal microscope based on Ntegra Spectra (NT MDT) spectroscopy system. A lensed fiber was used to focus the YAG:Nd laser beam and pump the microdisk uniformly and a long working distance objective with piezo-driven mirrors was used to scan the disk and collect emission from the top. The light was detected by ANDOR InGaAs CCD detector in 1240−1300 nm spectral range.

RESULTS AND DISCUSSION

The micro-PL spectra of the microdisk laser obtained at different pump powers P are shown in Figure 3. First, we measured the μPL spectra of as-formed microdisk of circular shape (Figure 3a). Then, we measured the μPL spectra of the self-same disk after growing the nanoantenna on its side wall (Figure 3b). In both cases, we observe a series of narrow WGM lasing lines superimposed on broad InAs/InGaAs quantum dot emission. One can see that the nanoantenna weakly affects the position of the eigenmodes. A slight red-shift (~5 nm) of the lasing spectrum at pump power 2280 μW (Figure 3b) could be explained by an increase of the temperature of the sample.

To interpret the position of the peaks in the spectra, we solved the eigenvalue problem for the microdisk cavity on the substrate numerically by finite element method using COMSOL Multiphysics software. The problem has rotational symmetry (before growing the nanoantenna) and, therefore, the azimuthal dependence of the mode fields is given by $\exp(im\varphi)$. Index m is an azimuthal mode number, and φ is the azimuthal angle. Separation of the variables allows one to reduce the problem from 3D to 2D geometry. Details of the simulation technique are described in ref 54. The simulation includes the $AlGa_xO_y$ pedestal with a height of 400 nm (as

DOI: 10.1021/acsphotonics.6b00552
ACS Photonics XXXX, XXX, XXX−XXX

homogeneous material with a refractive index about 1.6), the GaAs microdisk cavity with a height of 350 nm (as homogeneous material with permittivity 11.4), and the surrounding air. The diameter of the microcavity and pedestal are supposed to be the same and equal to 6 μm. The low-index $AlGa_xO_y$ pedestal provides the effective optical insulation of the cavity from the substrate and excludes the effect of the latter on mode structure of the cavity and laser characteristics.

Comparison of the results of numerical simulations with experimental μPL spectra allows to identify three dominant lasing modes. The dominant WGM line at 1277 nm corresponds to the mode $TE_{40,1}$. The two other lines near 1290 and 1302 nm correspond to the modes $TM_{37,1}$ and $TE_{39,1}$, respectively. The distribution of the electric field intensity |**E**| for these modes is shown in Figure 3c.

Lasing operation is confirmed by the light−light characteristics of the 1277 nm ($TE_{40,1}$) mode (Figure 4a). As the pump power increases, the line width of the mode decreases down to ∼35 pm for as-formed microdisk and down to ∼40 pm for the microdisk with nanoantenna (Figure 4b). This corresponds to the $Q = \lambda/\Delta\lambda$ of 3.6×10^4 and 3.2×10^4, respectively. Thus, the nanoantenna does not affect the *Q*-factor significantly. The effect of the outcoupling improvement is similar to that observed for conventional lasers with Fabry−Perot resonators, when the slope efficiency increases as reflectivity of output mirror decreases. In other words, the nanoantenna makes higher the output loss of the microresonator. In its turn, this increases a fraction of input (pump) power, which converted into coherent emission that comes out of the microresonator. It should be noted that threshold power increases as a result of the nanoantenna presence, from 0.3 to 0.6 mW. It happens because the nanoantenna grown right up to the sidewall of the cavity introduces additional losses (scattering losses and absorption by Pt−C composite).

Near the lasing threshold P_{th}, the emission spectrum is multimode. With increasing pumping level, the dominant WGM line intensity grows and side mode suppression ratio (SMSR) for the as-formed microdisk laser reaches its maximum value of 10 dB at $P = 1.33 \times P_{th}$ (Figure 5, blue markers). At higher pump power ($1.7 \times P_{th}$), the intensity of the lasing mode starts to recede and subsequent longer wavelength mode builds-up, which leads to a decrease of the SMSR value. This effect is presumably caused by a decrease in gain at the wavelength of the WGM involved in lasing. The nanoantenna changes the behavior of the WGM cavity dramatically. We observe the increase in the maximal output light intensity by more than 20 times (Figure 4a). The increase is accompanied by the efficient suppression of side modes. The maximal SMSR of 24.7 dB is reached at $3.3 \times P_{th}$ (Figure 5). Pump level, at which the maximal WGM line intensity is achieved, shifts from $3.8 \times P_{th}$ to $5 \times P_{th}$.

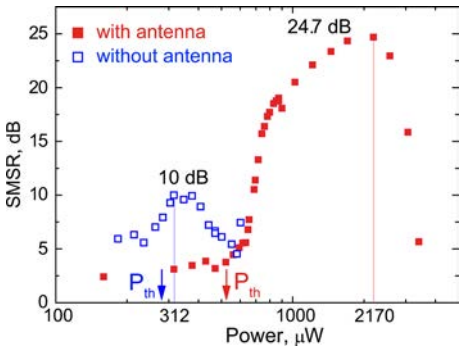

Figure 5. Side mode suppression ratio as a function of pump power for microdisk with and without nanoantenna. The maximal SMSR is achieved at the pump powers 312 and 2170 μW for the as-formed microdisk and the microdisk with the nanoantenna, respectively.

The distributions of the dominant mode intensity ($TE_{40,1}$) of the microdisk with and without the nanoantenna measured by the confocal scanning optical spectroscopy are shown in Figure 6a and b, respectively. The pump level is $1.5 \times P_{th}$ in both cases.

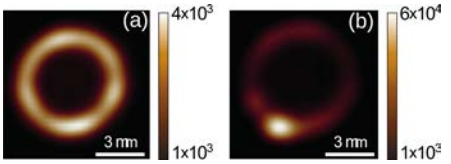

Figure 6. Emission patterns of the dominant mode ($TE_{40,1}$) obtained at pumping level above the threshold ($P \sim 1.5P_{th}$) of the microdisk with (a) and without nanoantenna (b).

The as-formed microdisk demonstrates nearly uniform (isotropic) emission distribution along its edge with a slight modulation, which does not exceed a factor of 2. It occurs due to the light scattering on the side wall roughness appeared during the lithography process. Figure 6b shows that the nanoantenna dramatically changes the intensity distribution of the dominant mode. A hotspot located at the position of the nanoantenna is now clearly visible. The intensity at the hotspot exceeds the intensity at other positions by an order of magnitude that confirms that the energy accumulated in the cavity is effectively outcoupled through the nanoantenna.

In order to explain the observed results and to gain deeper insight into the problem of light outcoupling from the microcavity through the nanoantenna we provide numerical simulations using CST Microwave Studio.

The data for the permittivity of the microdisk, the pedestal and the substrate we took from ref 55. The optical parameters of the Pt−C nanoantenna were extracted from the measurements of the volt-ampere characteristics under DC voltage (Figure 2). They show that the nanoantenna has metallic conductance comparable with the one of thin Pt films.[47,48] High frequency (optical) permittivity of Pt−C nanoantenna can be estimated from the static measurements in the scope of the Drude approach[56]

$$\varepsilon(\omega) = \varepsilon_\infty + \frac{4\pi i\sigma_s}{\omega(1 - i\tau\omega)} \quad (1)$$

Here, σ_s and τ are the static conductivity that we obtain from the DC voltage volt-ampere characteristics and the momentum relaxation time of electrons. In our calculations we put $\tau = 0.06$ ps and $\varepsilon_\infty = 5.4$.[57]

The distribution of electric field intensity in the system "microdisk+nanoantenna" for the mode $TE_{40,1}$ is shown in Figure 7a. One can see that the electromagnetic field around the nanoantenna is peculiar to surface plasmon polariton. It weakly penetrates inside the nanoantenna, exponentially decreases away from its surface, and propagates along the wire. So, it is possible to assert that Pt−C wire plays the role of a plasmonic waveguide. Surface plasmon polariton is excited by WGM, then it propagates along the nanoantenna and scatters at its tip providing vertically directed laser emission. Map of the Poynting vector (see Figure 7b) shows that electromagnetic

DOI: 10.1021/acsphotonics.6b00552
ACS Photonics XXXX, XXX, XXX−XXX

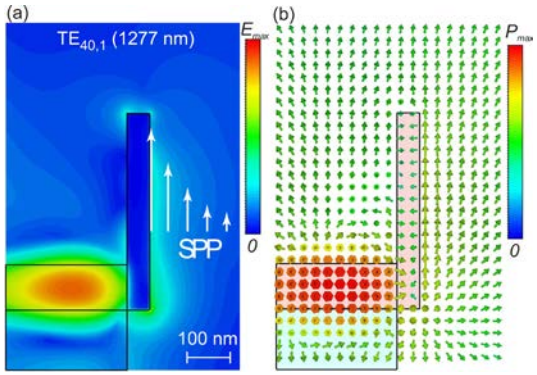

Figure 7. (a) Distribution of electric field amplitude |**E**| (in logarithmic scale) and (b) map of the Poynting vector (arrows) in the vicinity of the Pt−C nanoantenna for the dominant WGM ($TE_{40,1}$, λ = 1277 nm).

energy propagates predominantly in the vertical direction along the wire. Without the nanoantenna, the emission is mainly concentrated in the plane of the microdisk and vertical light emission occurs only due to the roughnesses and defects of the top surface.[58−60]

CONSLUSION

We have proposed and implemented a novel method for efficient WGM outcoupling from microcavities providing directional emission while keeping the Q-factor of the cavity nearly undisturbed (over 3×10^4). Within this method, the energy accumulated in the microcavity outcouples via a plasmonic Pt−C nanoantenna grown on the side wall of the microdisk by electron beam assisted deposition. We have demonstrated a SMSR increment of up to 24 dB and the dominant mode intensity enhancement by 20 times in room temperature spectra of 6 μm diameter QD microdisk lasers. The emission pattern demonstrates a bright spot at the position of the nanoantenna. The presented concept provide the ability to control spectrum and emission directivity of microdisk lasers that is very promising for many practical applications from telecommunication technologies to biosensing.

ASSOCIATED CONTENT

Supporting Information

The Supporting Information is available free of charge on the ACS Publications website at DOI: 10.1021/acsphotonics.6b00552.

Supporting Figures S1−S3 (PDF).

AUTHOR INFORMATION

Corresponding Author

*E-mail: a.bogdanov@metalab.ifmo.ru.

ORCID

Zarina F. Sadrieva: 0000-0001-8299-3226

Alexander E. Krasnok: 0000-0001-7419-781X

Andrey A. Bogdanov: 0000-0002-8215-0445

Notes

The authors declare no competing financial interest.

ACKNOWLEDGMENTS

The work is supported by the Skolkovo Foundation (Grant Agreement for Russian educational and scientific organization no.6 dd. 30.12.2015). Y.S.P. acknowledges the Government of St. Petersburg and The Committee on Science and Higher Education. A.B.B. acknowledges the RFBR (17-02-01331, 16-37-60064), the Ministry of Education and Science of the Russian Federation (Zadanie No.3.1668.2017). We are greatly thankful to I. S. Sinev for useful discussion, proofreading, and help with optical measurements.

REFERENCES

(1) Novotny, L.; van Hulst, N. Antennas for light. *Nat. Photonics* **2011**, *5*, 83−90.

(2) Giannini, V.; Fernandez-Dominguez, A. I.; Heck, S. C.; Maier, S. A. Plasmonic Nanoantennas: Fundamentals and Their Use in Controlling the Radiative Properties of Nanoemitters. *Chem. Rev.* **2011**, *111*, 3888−3912.

(3) Biagioni, P.; Huang, J.-S.; Hecht, B. Nanoantennas for visible and infrared radiation. *Rep. Prog. Phys.* **2012**, *75*, 024402.

(4) Maksymov, I. S.; Staude, I.; Miroshnichenko, A. E.; Kivshar, Y. S. Optical Yagi-Uda nanoantennas. *Nanophotonics* **2012**, *1*, 65−81.

(5) Krasnok, A. E.; Maksymov, I. S.; Denisyuk, A. I.; Belov, P. A.; Miroshnichenko, A. E.; Simovski, C. R.; Kivshar, Y. S. Optical nanoantennas. *Phys.-Usp.* **2013**, *56*, 539−564.

(6) Ahmed, A.; Gordon, R. Directivity Enhanced Raman Spectroscopy Using Nanoantennas. *Nano Lett.* **2011**, *11*, 1800−1803.

(7) Chen, P.-Y.; Argyropoulos, C.; Alu, A. Enhanced nonlinearities using plasmonic nanoantennas. *Nanophotonics* **2012**, *1*, 221−233.

(8) Chen, P.-Y.; Argyropoulos, C.; D'Aguanno, G.; Alu, A. Enhanced Second-Harmonic Generation by Metasurface Nanomixer and Nanocavity. *ACS Photonics* **2015**, *2*, 1000−1006.

(9) Mesch, M.; Metzger, B.; Hentschel, M.; Giessen, H. Nonlinear Plasmonic Sensing. *Nano Lett.* **2016**, *16*, 3155−3159.

(10) Ni, X.; Emani, N. K.; Kildishev, A. V.; Boltasseva, A.; Shalaev, V. M. Broadband Light Bending with Plasmonic Nanoantennas. *Science* **2012**, *335*, 427.

(11) Guo, R.; Decker, M.; Setzpfandt, F.; Staude, I.; Neshev, D. N.; Kivshar, Y. S. Plasmonic Fano Nanoantennas for On-Chip Separation of Wavelength-Encoded Optical Signals. *Nano Lett.* **2015**, *15*, 3324−3328.

(12) Shiigi, H.; Kinoshita, T.; Fukuda, M.; Le, D. Q.; Nishino, T.; Nagaoka, T. Nanoantennas as Biomarkers for Bacterial Detection. *Anal. Chem.* **2015**, *87*, 4042−4046.

(13) Coenen, T.; Vesseur, E. J. R.; Polman, A.; Koenderink, A. F. Directional Emission from Plasmonic Yagi-Uda Antennas Probed by Angle-Resolved Cathodoluminescence Spectroscopy. *Nano Lett.* **2011**, *11*, 3779−3784.

(14) Livneh, N.; Harats, M. G.; Istrati, D.; Eisenberg, H. S.; Rapaport, R. Highly Directional Room-Temperature Single Photon Device. *Nano Lett.* **2016**, *16*, 2527−2532.

(15) Choudhury, S. D.; Badugu, R.; Lakowicz, J. R. Directing Fluorescence with Plasmonic and Photonic Structures. *Acc. Chem. Res.* **2015**, *48*, 2171−2180.

(16) Srinivasan, K.; Borselli, M.; Painter, O.; Stintz, A.; Krishna, S. Cavity Q, mode volume, and lasing threshold in small diameter AlGaAs microdisks with embedded quantum dots. *Opt. Express* **2006**, *14*, 1094.

(17) Dettmann, C. P.; Morozov, G. V.; Sieber, M.; Waalkens, H. Unidirectional Emission from Circular Dielectric Microresonators with a Point Scatterer. *Phys. Rev. A: At., Mol., Opt. Phys.* **2009**, *80*, 063813.

(18) Apalkov, V. M.; Raikh, M. E. Directional emission from a microdisk resonator with a linear defect. *Phys. Rev. B: Condens. Matter Mater. Phys.* **2004**, *70*, 195317.

(19) Tulek, A.; Vardeny, Z. Unidirectional laser emission from π-conjugated polymer microcavities with broken symmetry. *Appl. Phys. Lett.* **2007**, *90*, 161106.

(20) Wiersig, J.; Hentschel, M. Unidirectional light emission from high-Q modes in optical microcavities. *Phys. Rev. A: At., Mol., Opt. Phys.* **2006**, *73*, 031802.

DOI: 10.1021/acsphotonics.6b00552
ACS Photonics XXXX, XXX, XXX−XXX

(21) Polubavkina, Y. S.; Kryzhanovskaya, N.; Moiseev, E.; Kulagina, M.; Mukhin, I.; Komissarenko, F.; Zadiranov, Y. M.; Maximov, M.; Krasnok, A.; Bogdanov, A.; et al. Improved emission outcoupling from microdisk laser by Si nanospheres. *J. Phys.: Conf. Ser.* **2016**, *741*, 012158.
(22) Serpengüzel, A.; Griffel, G.; Arnold, S. Excitation of resonances of microspheres on an optical fiber. *Opt. Lett.* **1995**, *20*, 654−656.
(23) Choi, S. J.; Djordjev, K.; Choi, S. J.; Dapkus, P. D. Microdisk lasers vertically coupled to output waveguides. *IEEE Photonics Technol. Lett.* **2003**, *15*, 1330−1332.
(24) Cai, M.; Painter, O.; Vahala, K. J. Observation of critical coupling in a fiber taper to a silica-microsphere whispering-gallery mode system. *Phys. Rev. Lett.* **2000**, *85*, 74.
(25) Koseki, S.; Zhang, B.; De Greve, K.; Yamamoto, Y. Monolithic integration of quantum dot containing microdisk microcavities coupled to air-suspended waveguides. *Appl. Phys. Lett.* **2009**, *94*, 051110.
(26) Shah Hosseini, E.; Yegnanarayanan, S.; Atabaki, A. H.; Soltani, M.; Adibi, A. Systematic design and fabrication of high-Q single-mode pulley-coupled planar silicon nitride microdisk resonators at visible wavelengths. *Opt. Express* **2010**, *18*, 2127.
(27) Rowland, D.; Love, J. Evanescent wave coupling of whispering gallery modes of a dielectric cylinder. *IEE Proc.-J: Optoelectron.* **1993**, *140*, 177.
(28) Liu, Y.; Chang, T.; Craig, A. E. Coupled mode theory for modeling microring resonators. *Opt. Eng.* **2005**, *44*, 084601.
(29) Song, Q. H.; Ge, L.; Stone, A. D.; Cao, H.; Wiersig, J.; Shim, J.-B.; Unterhinninghofen, J.; Fang, W.; Solomon, G. S. Directional Laser Emission from a Wavelength-Scale Chaotic Microcavity. *Phys. Rev. Lett.* **2010**, *105*, 103902.
(30) Albert, F.; Hopfmann, C.; Eberspacher, A.; Arnold, F.; Emmerling, M.; Schneider, C.; Hofling, S.; Forchel, A.; Kamp, M.; Wiersig, J.; et al. Directional whispering gallery mode emission from Limacon-shaped electrically pumped quantum dot micropillar lasers. *Appl. Phys. Lett.* **2012**, *101*, 021116.
(31) Wang, Q. J.; Yan, C.; Yu, N.; Unterhinninghofen, J.; Wiersig, J.; Pflugl, C.; Diehl, L.; Edamura, T.; Yamanishi, M.; Kan, H.; et al. Whispering-gallery mode resonators for highly unidirectional laser action. *Proc. Natl. Acad. Sci. U. S. A.* **2010**, *107*, 22407−22412.
(32) Hahn, K. H.; Tan, M. R.; Wang, S.-Y. Optical communication with vertical-cavity surface-emitting laser operating in multiple transverse modes. U.S. Patent US5,359,447, 1994.
(33) Rodes, R.; Estaran, J.; Li, B.; Muller, M.; Jensen, J. B.; Gruendl, T.; Ortsiefer, M.; Neumeyr, C.; Rosskopf, J.; Larsen, K. J.; et al. 100 Gb/s single VCSEL data transmission link. *National Fiber Optic Engineers Conference*; OSA Publishing, 2012; pp 1−3. .
(34) Wiedenmann, D.; King, R.; Jung, C.; Jäger, R.; Michalzik, R.; Schnitzer, P.; Kicherer, M.; Ebeling, K. J. Design and analysis of single-mode oxidized VCSELs for high-speed optical interconnects. *IEEE J. Sel. Top. Quantum Electron.* **1999**, *5*, 503−511.
(35) Hurtado, A.; Henning, I. D.; Adams, M. J. Optical neuron using polarisation switching in a 1550nm-VCSEL. *Opt. Express* **2010**, *18*, 25170−25176.
(36) Koyama, F. Recent advances of VCSEL photonics. *J. Lightwave Technol.* **2006**, *24*, 4502−4513.
(37) Tsai, C.-L.; Lee, F.-M.; Cheng, F.-Y.; Wu, M.-C.; Ko, S.-C.; Wang, H.-L.; Ho, W.-J. Silicon oxide-planarized single-mode 850-nm VCSELs with TO package for 10 Gb/s data transmission. *IEEE Electron Device Lett.* **2005**, *26*, 304−307.
(38) Karinou, F.; Stojanovic, N.; Prodaniuc, C.; Agustin, M.; Kropp, J.-R.; Ledentsov, N. N. Solutions for 100/400-Gb/s Ethernet Systems based on Multimode Photonic Technologies. *J. Lightwave Technol.* **2016**, 1.
(39) Vollmer, F.; Arnold, S. Whispering-gallery-mode biosensing: label-free detection down to single molecules. *Nat. Methods* **2008**, *5*, 591−596.
(40) Savchenkov, A. A.; Matsko, A. B.; Mohageg, M.; Maleki, L. Ringdown spectroscopy of stimulated Raman scattering in a whispering gallery mode resonator. *Opt. Lett.* **2007**, *32*, 497−499.
(41) Maximov, M. V.; Kryzhanovskaya, N. V.; Nadtochiy, A. M.; Moiseev, E. I.; Shostak, I. I.; Bogdanov, A. A.; Sadrieva, Z. F.; Zhukov, A. E.; Lipovskii, A. A.; Karpov, D. V.; et al. Ultrasmall microdisk and microring lasers based on InAs/InGaAs/GaAs quantum dots. *Nanoscale Res. Lett.* **2014**, *9*, 657.
(42) Zhukov, A. E.; Kryzhanovskaya, N. V.; Maximov, M. V.; Lipovskii, A. A.; Savelyev, A. V.; Bogdanov, A. A.; Shostak, I. I.; Moiseev, E. I.; Karpov, D. V.; Laukkanen, J.; et al. Lasing in microdisks of ultrasmall diameter. *Semiconductors* **2014**, *48*, 1626−1630.
(43) Backes, S. A.; Cleaver, J. R. A.; Heberle, A. P.; Kohler, K. Microdisk laser structures for mode control and directional emission. *J. Vac. Sci. Technol., B: Microelectron. Process. Phenom.* **1998**, *16*, 3817.
(44) Kryzhanovskaya, N. V.; Mukhin, I. S.; Moiseev, E. I.; Shostak, I. I.; Bogdanov, A. A.; Nadtochiy, A. M.; Maximov, M. V.; Zhukov, A. E.; Kulagina, M. M.; Vashanova, K. A.; et al. Control of emission spectra in quantum dot microdisk/microring lasers. *Opt. Express* **2014**, *22*, 25782−25787.
(45) Bogdanov, A. A.; Mukhin, I. S.; Kryzhanovskaya, N. V.; Maximov, M. V.; Sadrieva, Z. F.; Kulagina, M. M.; Zadiranov, Y. M.; Lipovskii, A. A.; Moiseev, E. I.; Kudashova, Y. V.; et al. Mode selection in InAs quantum dot microdisk lasers using focused ion beam technique. *Opt. Lett.* **2015**, *40*, 4022.
(46) Blokhin, S. A.; Kryzhanovskaya, N. V.; Gladyshev, A. G.; Maleev, N. A.; Kuz'menkov, A. G.; Arakcheeva, E. M.; Tanklevskaya, E. M.; Zhukov, A. E.; Vasil'ev, A. P.; Semenova, E. S.; et al. Optical studies of asymmetric-waveguide submonolayer InGaAs QD microdisks formed by selective oxidation. *Semiconductors* **2006**, *40*, 476−480.
(47) Notargiacomo, A.; Di Gaspare, L.; Evangelisti, F. Ion beam assisted processes for Pt nanoelectrode fabrication onto 1-D nanostructures. *Superlattices Microstruct.* **2009**, *46*, 149−152.
(48) Smith, S.; Walton, A. J.; Bond, S.; Ross, A. W.; Stevenson, J. T. M.; Gundlach, A. M. Electrical characterization of platinum deposited by focused ion beam. *IEEE Trans. Semicond. Manuf.* **2003**, *16*, 199−206.
(49) Ballestar, A.; Esquinazi, P. Transport characteristics of focused beam deposited nanostructures. *Nanofabrication* **2015**, *2*, 1−18.
(50) Li, P. G.; Jin, A. Z.; Tang, W. H. Pt/Ga/C and Pt/C composite nanowires fabricated by focused ion and electron beam induced deposition. *Phys. Status Solidi A* **2006**, *203*, 282−286.
(51) Peñate-Quesada, L.; Mitra, J.; Dawson, P. Non-linear electronic transport in Pt nanowires deposited by focused ion beam. *Nanotechnology* **2007**, *18*, 215203.
(52) Wiedemair, J.; Menegazzo, N.; Pikarsky, J.; Booksh, K. S.; Mizaikoff, B.; Kranz, C. Novel electrode materials based on ion beam induced deposition of platinum carbon composites. *Electrochim. Acta* **2010**, *55*, 5725−5732.
(53) Stanford, M. G.; Lewis, B. B.; Noh, J. H.; Fowlkes, J. D.; Roberts, N. A.; Plank, H.; Rack, P. D. Purification of Nanoscale Electron-Beam-Induced Platinum Deposits via a Pulsed Laser-Induced Oxidation Reaction. *ACS Appl. Mater. Interfaces* **2014**, *6*, 21256−21263.
(54) Oxborrow, M. Traceable 2-D Finite-Element Simulation of the Whispering-Gallery Modes of Axisymmetric Electromagnetic Resonators. *IEEE Trans. Microwave Theory Tech.* **2007**, *55*, 1209−1218.
(55) Siklitsky, V. New Semiconductor Materials. Characteristics and Properties. 1998; http://www.ioffe.ru/SVA/NSM/.
(56) Jackson, J. D. *Classical Electrodynamics*; Wiley: New York, 1999.
(57) Ordal, M. A.; Long, L. L.; Bell, R. J.; Bell, S. E.; Bell, R. R.; Alexander, J. R.; Ward, C. A. Optical properties of the metals Al, Co, Cu, Au, Fe, Pb, Ni, Pd, Pt, Ag, Ti, and W in the infrared and far infrared. *Appl. Opt.* **1983**, *22*, 1099.
(58) Rahachou, A. I.; Zozoulenko, I. V. Effects of boundary roughness on a Q factor of whispering-gallery-mode lasing microdisk cavities. *J. Appl. Phys.* **2003**, *94*, 7929.
(59) Borselli, M.; Srinivasan, K.; Barclay, P. E.; Painter, O. Rayleigh scattering, mode coupling, and optical loss in silicon microdisks. *Appl. Phys. Lett.* **2004**, *85*, 3693.

DOI: 10.1021/acsphotonics.6b00552
ACS Photonics XXXX, XXX, XXX−XXX

(60) Borselli, M.; Johnson, T. J.; Painter, O. Beyond the Rayleigh scattering limit in high- Q silicon microdisks: theory and experiment. *Opt. Express* **2005**, *13*, 1515−1530.

DOI: 10.1021/acsphotonics.6b00552
ACS Photonics XXXX, XXX, XXX−XXX